Influences of Exfoliated Graphite on Structures, Thermal Stability, Mechanical Modulus, and Electrical Resistivity of Poly(butylene terephthalate)

Meilu Li and Young Gyu Jeong

Department of Materials Design Engineering, Kumoh National Institute of Technology, Gumi, Gyeongbuk 730-701, Republic of Korea

Received 27 June 2011; accepted 8 November 2011
DOI 10.1002/app.36465
Published online 1 February 2012 in Wiley Online Library (wileyonlinelibrary.com).

ABSTRACT: We report structural features and multifunctional properties of nanocomposites based on poly(butylene terephthalate) (PBT) and exfoliated graphite (EG), which are manufactured by melt-compounding technique. Scanning electron microscope and X-ray diffraction data exhibit that graphene platelets of EG are well dispersed and exfoliated in the PBT matrix even at high EG content of 7.0 wt %. Raman spectra support that graphene platelets of EG are interacted specifically with phenyl rings of PBT chains at nanocomposite interfaces. DSC cooling and following heating thermograms of the nanocomposites demonstrate that graphene platelets of EG play a role as effective nucleating agents for PBT α-phase crystals and thus lead to accelerating the overall crystallization of the nanocomposites. Thermal stability of PBT/EG nanocomposites is improved substantially due to the gas barrier effect of graphene platelets of EG dispersed in the PBT matrix, especially at the active oxygen gas condition. Dynamic mechanical modulus of the nanocomposites is also enhanced significantly with increasing the EG content. The electrical volume resistivity of the nanocomposites is decreased dramatically from $\sim 10^{18}$ to $\sim 10^{6}$ Ω cm by forming the electrical conduction path at a certain EG content between 3 and 5 wt %. J Appl Polym Sci 125: E532–E540, 2012

Key words: poly(butylene terephthalate); exfoliated graphite; thermal stability; mechanical modulus; electrical resistivity

INTRODUCTION

Poly(butylene terephthalate) (PBT) is a thermoplastic and semicrystalline polymer and, as a member of the poly(alkylene terephthalate) family, is derived from a polycondensate of terephthalic acid with 1,4-butanediol. PBT has relatively rapid crystallization rate and high elasticity compared with poly(ethylene terephthalate) (PET), but it has somewhat lower strength and stiffness than PET. Nonetheless, because of its combining excellent mechanical properties with robust chemical resistance and dimensional stability, PBT has been widely used for an engineering thermoplastic[1–3] or for a component in blends,[4–9] copolymers,[10–13] and composites.[14–17] However, for high-performance applications, thermal and mechanical properties of PBT need to be enhanced. As PBT is also an intrinsically insulating material, electrical resistivity of PBT must be highly lowered in advanced applications requiring electrostatic and/or electromagnetic dissipation.

Graphene is an important allotrope of carbon, whose structure is one-atom-thick planar sheet of sp^2-bonded carbon atoms that are densely packed in a honeycomb crystal lattice. Graphene platelets are stacked to form three-dimensional graphite, which is naturally abundant, with an interplanar spacing of 0.335 nm. The interlayer bonds between graphene platelets are rather weak, as they are held together by van der Waals interactions. As the recent discovery of graphene[18] with its outstanding physical properties such as electrical conductivity of $\sim 10^4$ S/cm,[18,19] in-plane elastic modulus of $\sim$ 1 TPa,[20] and thermal stability, graphene platelet has been considered as an ideal reinforcing nanoscale filler for improving thermal, mechanical, and electrical properties of polymeric materials.[21–29] Nonetheless, PBT-based nanocomposites reinforced with graphene platelets have not been studied until now.

In this study, we have manufactured a series of PBT-based nanocomposites reinforced with graphene platelets via melt-compounding for the first time and investigated the effects of graphene platelets on melting/crystallization behavior, thermal stability, mechanical modulus, and electrical resistivity of PBT by adopting differential scanning calorimetry,

Correspondence to: Y. G. Jeong (ygjeong@kumoh.ac.kr).
Contract grant sponsor: National Research Foundation of Korea (NRF; Basic Science Program), Ministry of Education, Science and Technology; contract grant number: 2010-0011176.

thermogravimetric analysis, dynamic mechanical analysis, and electrical resistivity measurement, respectively. For the purpose, exfoliated graphite (EG), which consists of disordered graphene platelets, is prepared by the rapid thermal expansion and reduction of graphite oxide obtained from the acid-treatment of highly crystalline natural graphite flakes. Structural and morphological features of PBT nanocomposites with various EG contents are also examined by using X-ray diffraction method and scanning electron microscopy. In addition, Raman spectroscopic analysis of the nanocomposites is carried out to understand the interfacial interaction between graphene platelets of EG and PBT chains.

EXPERIMENTAL

Materials

A commercially available PBT chips with intrinsic viscosity of 1.25 dL/g was used as a polymer matrix. Pristine natural graphite (grade 3061) with an average diameter of 500 μm was purchased from Sigma-Aldrich (St. Louis, MO). EG as reinforcing nanofiller was prepared from pristine natural graphite via the acid-treatment and following thermal expansion.[30–32] The detailed preparation procedure of EG used in this study was described in the previous report.[33]

Preparation of PBT/EG nanocomposites

PBT-based nanocomposites containing various EG contents were prepared by melt-compounding method. Before melt-compounding, all the components were dried in vacuum at 80°C for 24 h. The predetermined EG content was mixed mechanically with PBT powder in the solid state for 3 min. The EG contents in the mixtures were adjusted to be 0.0, 0.1, 0.3, 0.5, 0.7, 1.0, 3.0, 5.0, and 7.0 wt %. The solid mixtures were then melt-extruded through a corotating twin-screw extruder (BK-11, Bowtek, Republic of Korea) with a screw length of 440 mm and screw diameter of 11 mm. The temperature profile of the extruder from Zone 1 to 6 was controlled between 230 and 245°C. The screw speed was fixed at 170 rpm. The extruded strands were cooled into a water bath, chopped into pellets, and dried under vacuum at 80°C for 24 h. For structural and property characterization, melt-quenched film samples of 0.20 mm thickness were prepared by compression-molding the pellets in a hot-plate at 245°C and 18 MPa for 4 min, quenching into an iced-water bath, and then drying in a vacuum oven at 30°C overnight.

Characterization of PBT/EG nanocomposites

The dispersion state of graphene platelets of EG in the nanocomposites was characterized by using a scanning electron microscope (SEM, JEOL JSM-6380LV). For SEM images of the nanocomposites, the composite films were cryogenically fractured in a liquid nitrogen bath and then coated with gold/palladium.

The structural order of nanocomposite films with various EG contents was investigated by adopting X-ray diffraction method. X-ray diffraction patterns were obtained with a Rigaku X-ray diffractometer with Ni-filtered Cu-Kα radiation (40 kV and 150 mA) at a scanning rate of 2°/min.

The interfacial interaction between PBT and EG in the nanocomposites was characterized by using Raman spectroscopy (Renishaw, System 1000) with an excitation wavelength of He-Ne laser 514 nm. Melting and crystallization behaviors of the nanocomposites were examined by differential scanning calorimetry (Diamond DSC, Perkin Elmer). All measurements were performed under nitrogen gas condition at a heating/cooling rate of 10°C/min.

Thermal stability of PBT/EG nanocomposites was investigated as a function of EG content by using a thermogravimetric analyzer (TGA, TA Q500) under nitrogen or oxygen gas condition at a heating rate of 20°C/min.

Dynamic mechanical properties of the nanocomposite films with dimensions of $35.0 \times 5.0 \times 0.2$ mm^3 were examined with a dynamic mechanical analyzer (DMA, TA Q800) under the tensile mode from 0 to 220°C at a heating rate of 2°C/min and a frequency of 1 Hz.

Electrical properties of the nanocomposites were evaluated by measuring their electrical volume resistivity with aid of an electrometer high resistance meter and a resistivity test fixture (6517A, Keithley Instruments).

RESULTS AND DISCUSSION

Structural and morphological characterization

Figure 1 exhibits X-ray diffraction patterns and SEM images of pristine natural graphite flakes and EG prepared in this study. The original graphite flakes were characterized to have average diameter and thickness of $\sim$ 500 and $\sim$ 20 μm, respectively. X-ray diffraction pattern of the original graphite flakes showed a strong diffraction peak at $2\theta = 26.5°$, which is corresponding to the graphene interlayer distance of 0.336 nm. It supports that the original graphite flakes have well-ordered structures. On the other hand, the graphene platelets of EG, which was obtained by the acid-treatment of the original graphite flakes and the rapid thermal heating, did not show any diffraction peak in X-ray diffraction pattern. It indicates that the natural graphite flakes are highly expanded along their thickness direction

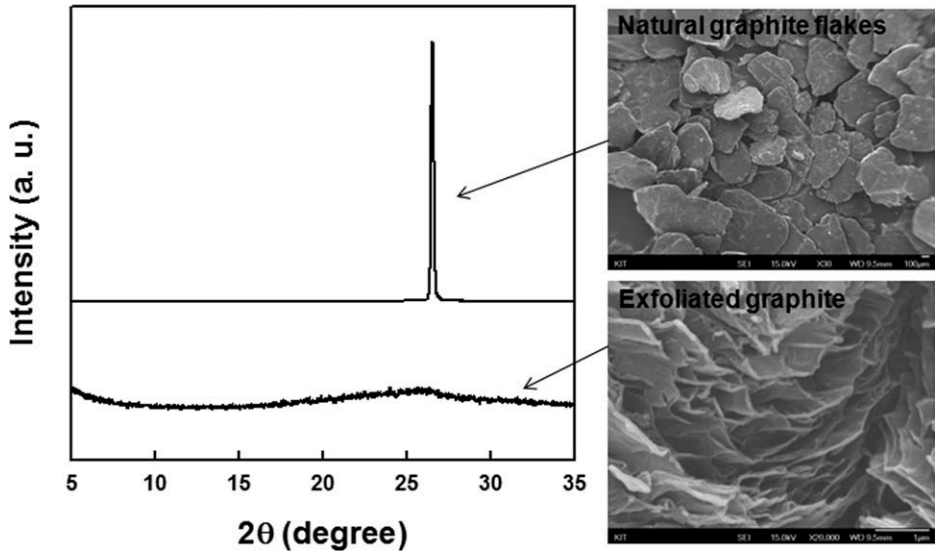

Figure 1 X-ray diffraction patterns and SEM images of natural graphite flakes and exfoliated graphite (EG). The EG was prepared by an acid-treatment and rapid thermal exfoliation of natural graphite flakes.

during the rapid thermal treatment and thus exfoliated, as confirmed by the SEM image of EG.

To characterize the dispersion state of EG in the PBT matrix, the cryogenically fractured surfaces of neat PBT and PBT/EG nanocomposites were examined by using SEM, as can be seen in Figure 2. The neat PBT exhibits quite even and smooth surface, indicating a typical brittle failure [Fig. 2(A)]. In cases of PBT/EG nanocomposites, much rougher fractured surfaces were seen on adding graphene platelets in the PBT matrix, as shown in Figure 2(B–F). Although the degree of fractured surface roughness increased with increasing the EG content in the nanocomposites, no agglomerated domains of graphene platelets of EG were observed even for the nanocomposite with high EG content of 7.0 wt %. It suggests that graphene platelets of EG were well delaminated and dispersed in the PBT matrix due to the high shear force generated during the melt-compounding.

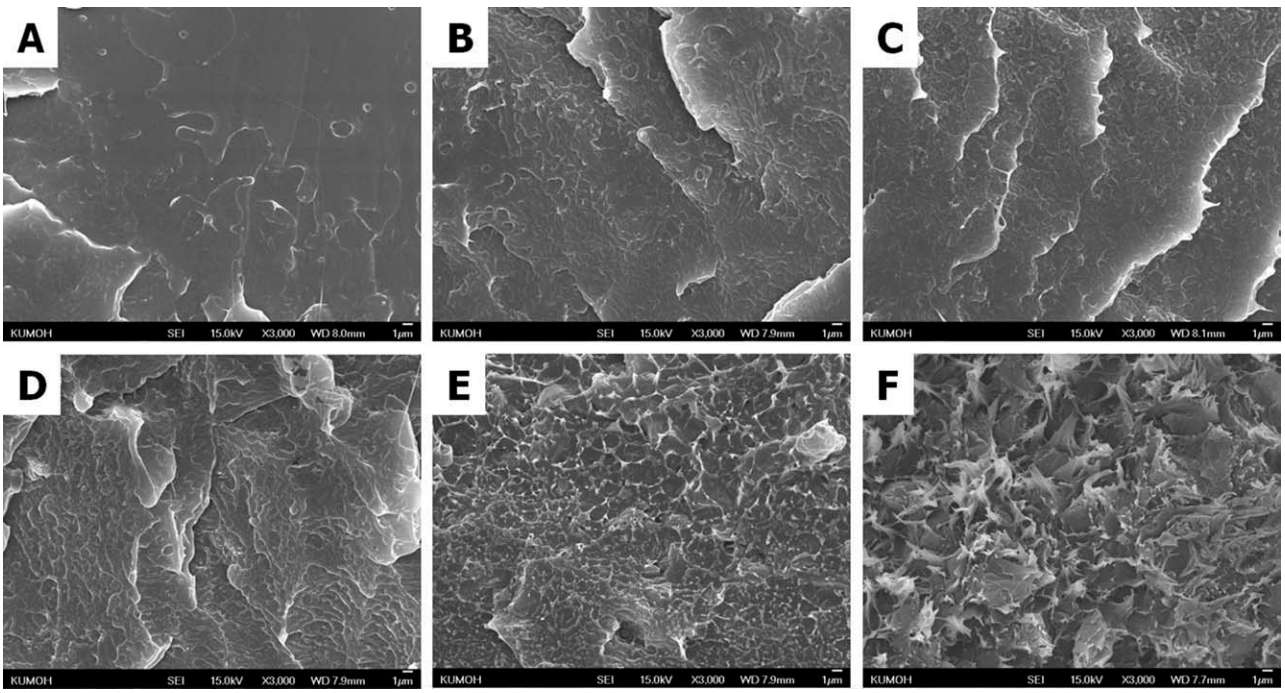

Figure 2 SEM images the cryogenically fractured surfaces for the neat PBT and PBT/EG nanocomposites with various EG contents: (A) neat PBT; (B) 0.3 wt % EG; (C) 0.7 wt % EG; (D) 1.0 wt % EG; (E) 3.0 wt % EG; (F) 7.0 wt % EG.

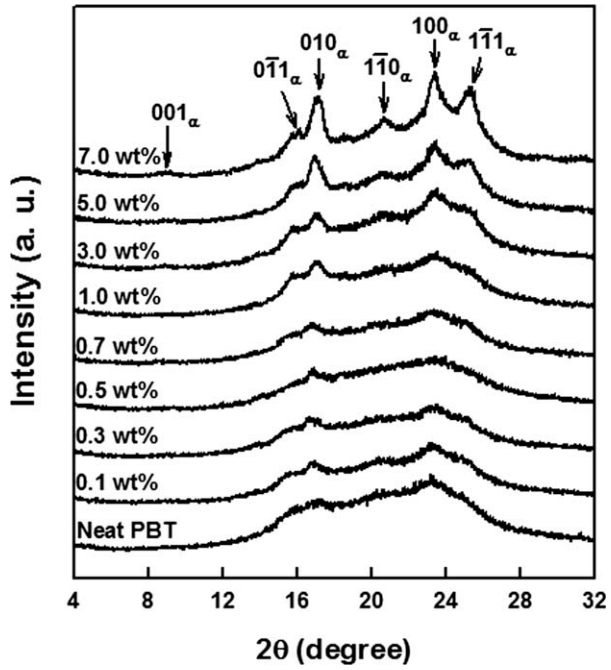

Figure 3 X-ray diffraction patterns of the melt-quenched neat PBT and PBT/EG nanocomposites with various EG contents.

X-ray diffraction patterns of the neat PBT and nanocomposites with various EG contents are shown in Figure 3. It was found that the pure PBT exhibited a broad amorphous hallow scatting without any strong crystalline diffraction peak. It demonstrates that the melt-quenched neat PBT film is mostly composed of amorphous phase. In contrast, the PBT/EG nanocomposites showed more intense crystalline diffraction peaks with increasing the EG content in the nanocomposites. The sharp diffraction peaks for the nanocomposites were identified to be caused by the α-phase crystals of PBT. It has been known that PBT has two crystal structures of α- and β-phases and that the reversible transition between two crystal phases takes place depending on the mechanical deformation, that is, the α-phase transforms to β-phase by applied stress for elongation and vice versa by relaxation.[34–37] Therefore, it is expected that graphene platelets of EG contribute dominantly to the formation of PBT α-phase crystals. On the other hand, it should be mentioned that there was no any characteristic diffraction peak of ordered graphene platelets or natural graphite. It supports the fact that graphene platelets of EG exist in an exfoliated and disordered state in the nanocomposites.

To understand the interfacial interaction between EG filler and PBT matrix, Raman spectra of the nanocomposite films were obtained, as shown in Figure 4. For the pristine EG, there are three common peaks, that is, a *D* peak at ~ 1350 cm^{-1}, a *G* peak at ~ 1587 cm^{-1}, and a *G′* peak at ~ 2700 cm^{-1} [Fig. 4(A-i)]. The *D* peak is defect-related and originates from the in-plane breathing mode of A_{1g} symmetry due to the presence of sixfold aromatic rings, whereas the *G* band is attributed to the first-order scattering of the E_{2g} vibrational model in graphene sheets.[38] Raman spectrum of the neat PBT is shown in Figure 4(A-a), which is consistent with the one in literature.[39] Strong bands at ~ 1611 and ~ 1717 cm^{-1} are identified to be the symmetric stretching vibrations of para-disubstituted benzene rings (C—C) and carbonyl groups (C=O), respectively. In cases of nanocomposites, overall Raman spectra are quite similar to that of the neat PBT, which is resulting from that the EG content in nanocomposites is relatively low [Fig. 4(A)]. Interestingly, it was found that the stretching vibration of benzene rings of PBT chains was slightly shifted to the higher

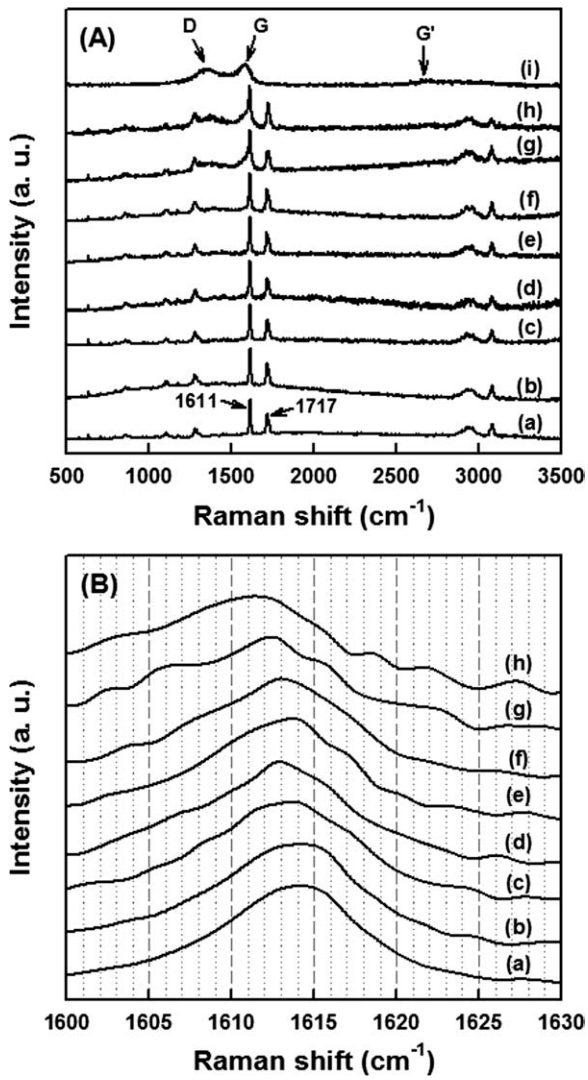

Figure 4 Raman spectra of for neat EG and PBT/EG nanocomposites with various EG contents: (a) neat PBT; (b) 0.1 wt % EG; (c) 0.3 wt % EG; (d) 0.5 wt % EG; (e) 0.7 wt % EG; (f) 1.0 wt % EG; (g) 3.0 wt % EG; (h) 5.0 wt % EG; (i) neat EG.

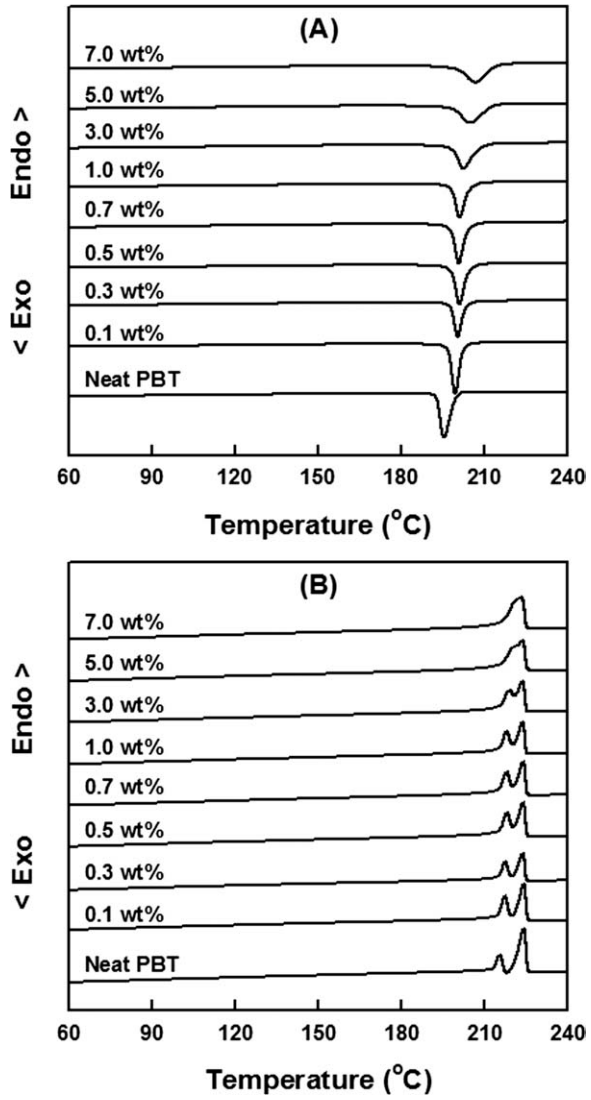

Figure 5 DSC cooling (A) and following heating (B) thermograms of the neat PBT and PBT/EG nanocomposites with various EG contents.

wavenumber from $\sim$ 1611 cm^{-1} for the neat PBT to $\sim$ 1614 cm^{-1} for the nanocomposite with 5 wt % EG [Fig. 4(B)]. This band shift to lower wavenumber with respect to the EG content of nanocomposites demonstrates that the phenyl rings of PBT chains are specifically interacting with graphene platelets of EG via aromatic–aromatic (π–π) interaction at the interface of nanocomposites.

Thermal analyses of PBT/EG nanocomposites

DSC cooling and heating thermograms of neat PBT and PBT/EG nanocomposites are shown in Figure 5. In the cooling thermograms [Fig. 5(A)], the melt-crystallization peaks shifted to higher temperatures from 196°C for the neat PBT to 207°C for the nanocomposite with 7.0 wt % EG, and they also became broader with the increment of EG content in the nanocomposites. This result indicates that the dispersed graphene platelets of EG act not only as seeds for faster formation of PBT nuclei but also as barriers to the formation of large PBT crystallites.[40] Nonetheless, graphene platelets of EG accelerates the overall melt-crystallization of PBT in the nanocomposites.

To characterize the melting behavior of PBT crystals formed during the cooling runs, the following heating thermograms were obtained, as can be seen in Figure 5(B). All the samples showed typical multiple melting endotherms, which are caused by the melting-recrystallization-remelting behavior.[41] In other words, the lower melting endotherm is associated with the melting of the original crystals developed during the melt-crystallization and the higher melting endotherm is related with the remelting of crystals formed by recrystallization during the heating process. It was also observed that the lower melting peaks are slightly shifted to higher temperatures from 215 to 223°C with increasing the EG content, while the higher melting peaks remained unchanged, regardless of the EG content in the nanocomposites. The shifts of the lower melting peaks to higher temperatures demonstrate that the original crystals developed during the cooling runs are thicker and more stable for the nanocomposites with higher EG contents. Overall, it is believed that the graphene platelets of EG dispersed in the PBT matrix contribute to the formation of stable and thick PBT crystals.

Thermal stability of PBT/EG nanocomposites under nitrogen and oxygen gas conditions was investigated using a thermogravimetric analyzer. TGA curves of the neat PBT and nanocomposites with different EG content under the nitrogen gas condition are shown in Figure 6(A). The characteristic thermal degradation temperatures for 5 and 30% weight loss ($T_{5\%}$ and $T_{30\%}$) under the nitrogen gas condition are also summarized in Table I. It was found that thermal degradation curves under the nitrogen gas condition are almost same for all the samples regardless of the EG content, except that the residues at 500°C are higher for the nanocomposites with higher EG contents. It means that the thermal stability of the nanocomposites under the nitrogen gas condition does not change much, regardless of the EG content. For instance, $T_{5\%}$ and $T_{30\%}$ values of the nanocomposite with 7 wt % EG are characterized to be 421 and 445°C, respectively, which are only 1.5 and 2°C higher than those of the neat PBT.

Thermo-oxidative degradation curves of the neat PBT and nanocomposites under the oxygen gas condition are shown in Figure 6(B). Unlike the nitrogen gas condition, it is apparent that the thermal stability of PBT/EG nanocomposites under the oxygen gas

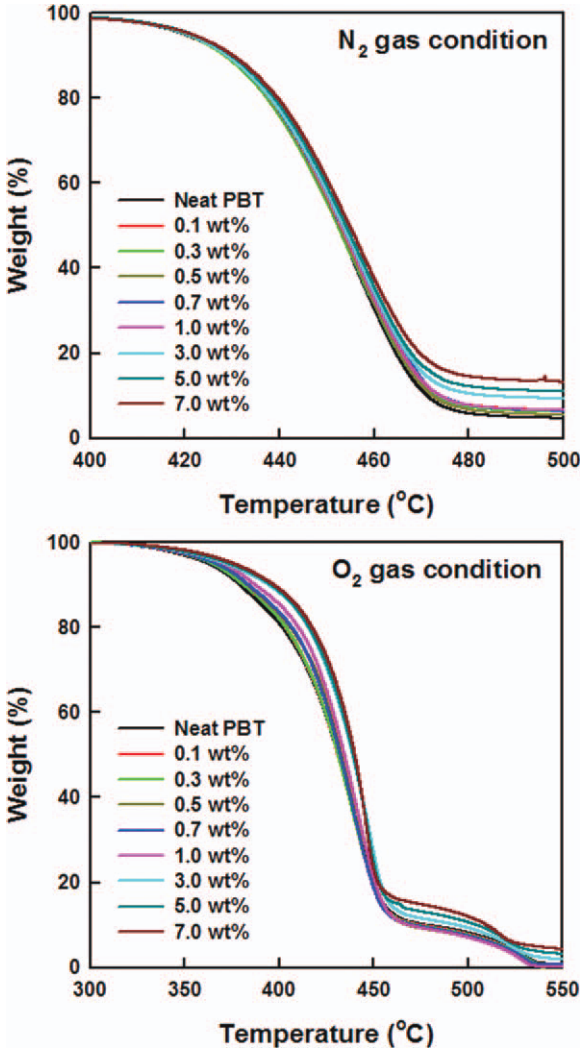

Figure 6 TGA thermograms of the neat PBT and PBT/EG nanocomposites with various EG contents examined under nitrogen and oxygen gas conditions. [Color figure can be viewed in the online issue, which is available at wileyonlinelibrary.com.]

condition is noticeably increased because of the presence of graphene platelets dispersed homogeneously in the PBT matrix. It was found that $T_{5\%}$ and $T_{30\%}$ values of the nanocomposite with 7 wt % EG are 13.6 and 12.7°C higher than those of the neat PBT, as listed in Table I. It is noticeable that the increment in $T_{5\%}$ and $T_{30\%}$ values of the nanocomposites under oxygen gas condition in comparison with the neat PBT is much larger than that under the inert nitrogen gas condition, although $T_{5\%}$ and $T_{30\%}$ values of the neat PBT and nanocomposites under the oxygen gas condition are far lower than the corresponding temperatures examined under the nitrogen gas condition. Recently, it has been reported that the gas permeation in graphene-based polymer nanocomposites is remarkably reduced, which is caused by the fact that the graphene platelets can serve as diffusion barriers in polymeric membranes.[42] Thus, it is reasonable to contend that the significant enhancement in thermal stability of PBT/EG nanocomposites under the oxygen gas condition is attributed to the barrier effect of graphene platelets to the active oxygen gas permeating through the PBT matrix.

Mechanical properties of PBT/EG nanocomposites

To investigate the effects of EG content on mechanical properties of the nanocomposites, dynamic mechanical measurements of the nanocomposites with various EG contents were carried out as a function of temperature, as can be seen in Figure 6. It was found that dynamic storage moduli of the nanocomposites were improved significantly at the glassy and rubbery regions, as the EG content increased [Fig. 7(A)]. This improvement in storage modulus can be attributed to the efficient transfer from PBT matrix to graphene platelets of EG, which is caused by the uniform distribution and good interfacial adhesion of graphene platelets in the PBT matrix. Meanwhile, the intensity of tan δ peaks decreased largely with increasing the EG content in the nanocomposites [Fig. 7(B)]. This result is originated from the fact that the increase in the dynamic storage moduli of the nanocomposites becomes larger compared with that of the dynamic loss modulus, as the EG content increases.

For randomly and discontinuously distributed planar fillers in the composites, Halpin–Tsai model can be used to predict the mechanical modulus of the composites,[43] which is written as

$$E_{\text{composite}} = \left[\frac{3}{8}\frac{1+(2d_{\text{EG}}/3t_{\text{EG}})\eta_{\text{L}}V_{\text{EG}}}{1-\eta_{\text{L}}V_{\text{EG}}} + \frac{5}{8}\frac{1+2\eta_{\text{T}}V_{\text{EG}}}{1-\eta_{\text{T}}V_{\text{EG}}}\right]E_{\text{PBT}} \quad (1)$$

TABLE I
Thermal Degradation Temperatures ($T_{5\%}$ and $T_{30\%}$) of 5 and 30% Weight Loss for the Neat PBT and PBT/EG Nanocomposites under Nitrogen and Oxygen Gas Conditions

		N_2 gas condition		O_2 gas condition	
Sample code	EG (wt %)	$T_{5\%}$ (°C)	$T_{30\%}$ (°C)	$T_{5\%}$ (°C)	$T_{30\%}$ (°C)
Neat PBT	0.0	419.7	443.6	362.8	415.4
PBT/EG	0.1	420.4	443.8	365.2	416.0
	0.3	420.2	443.6	364.9	416.2
	0.5	420.1	443.8	367.2	419.5
	0.7	420.4	444.0	366.7	418.7
	1.0	420.5	444.2	370.6	421.7
	3.0	420.3	444.2	371.8	426.0
	5.0	421.3	445.0	373.6	426.5
	7.0	421.4	445.7	376.4	428.1

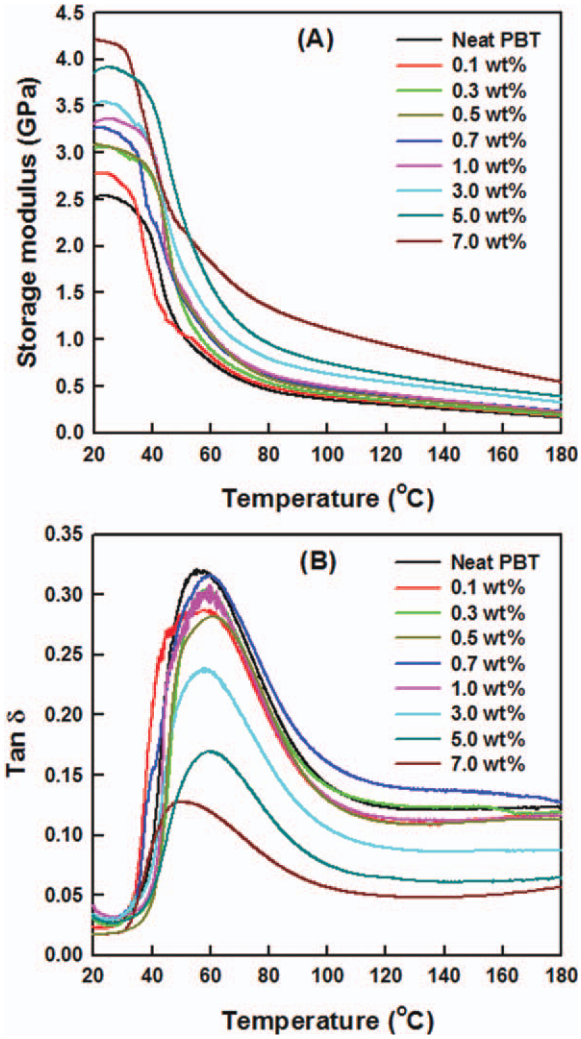

Figure 7 (A) dynamic storage modulus and (B) tan δ of the neat PBT and PBT/EG nanocomposites with various EG contents as a function of temperature. [Color figure can be viewed in the online issue, which is available at wileyonlinelibrary.com.]

$$\eta_L = \frac{(E_{EG}/E_{PBT}) - 1}{(E_{EG}/E_{PBT}) + (2d_{EG}/3t_{EG})}$$
$$\eta_T = \frac{(E_{EG}/E_{PBT}) - 1}{(E_{EG}/E_{PBT}) + 2}$$

where E_{EG} and E_{PBT} are the elastic moduli of graphene monolayer (1060 GPa)[20] and PBT matrix (2.47 GPa), respectively. d_{EG} is the average diameter (150 μm) of EG prepared in this study, and t_{EG} is the thickness (0.336 nm) of EG by assuming that the thickness of one graphene layer is equal to the interlayer separation in graphite. V_{EG} is the volume fraction of EG in the nanocomposites, which can be evaluated from the following equation

$$V_{EG} = \left[1 + \left(\frac{\rho_{EG}}{\rho_{PBT}}\right)\left(\frac{1 - m_{EG}}{m_{EG}}\right)\right]^{-1} \quad (2)$$

where m_{EG} is the mass fraction of EG. ρ_{EG} and ρ_{PBT} are the densities of graphite (1.9 g/cm^3) and PBT matrix (1.31 g/cm^3), respectively. Here, the density of EG is assumed to be same with that of the original graphite. The experimental dynamic storage moduli of the nanocomposites at 25°C were plotted as a function of the EG content, and they were compared with the moduli predicted from the Halpin–Tsai model, as shown in Figure 8. It was found that the experimental moduli of the nanocomposites increased rapidly with the EG content up to ~ 1 wt% and then increased slightly at higher EG contents up to ~ 7 wt%. The experimental modulus of the nanocomposite with 7.0 wt % EG content is nearly 66% higher than that of the neat PBT, which is ascribed to the effective reinforcement of graphene platelets of EG. On the other hand, although the experimental moduli of the nanocomposites were quite similar with the predicted moduli based on the Halpin–Tsai equation at lower EG contents less than 0.5 wt %, they were far lower than the predicted values at higher EG contents. It indicates that the mechanical reinforcing effect of graphene platelets is much dominant for the nanocomposites with lower EG contents. The large difference between experimental and predicted moduli of the nanocomposites with higher EG contents is believed to stem from the structural distortion and partial clustering of graphene platelets of EG in the matrix.

Electrical properties of PBT/EG nanocomposites

Figure 9 displays the electrical volume resistivity of the PBT/EG nanocomposites as a function of the EG content. The electrical volume resistivity of neat PBT

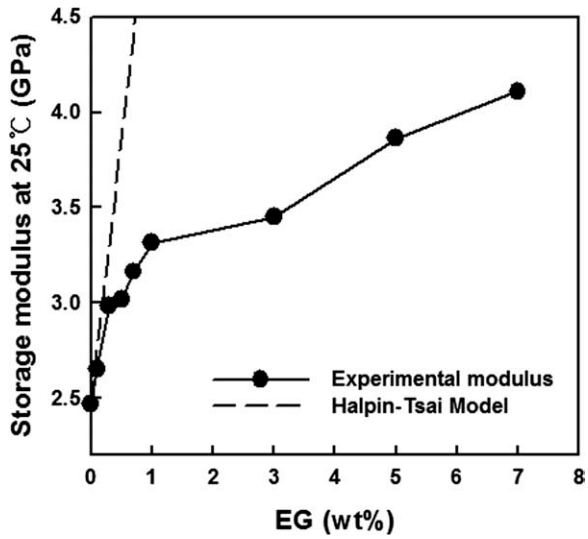

Figure 8 Dynamic storage moduli of PBT/EG nanocomposites at 25°C as a function of EG content. The dashed line denotes the moduli predicted by the Halpin–Tsai model.

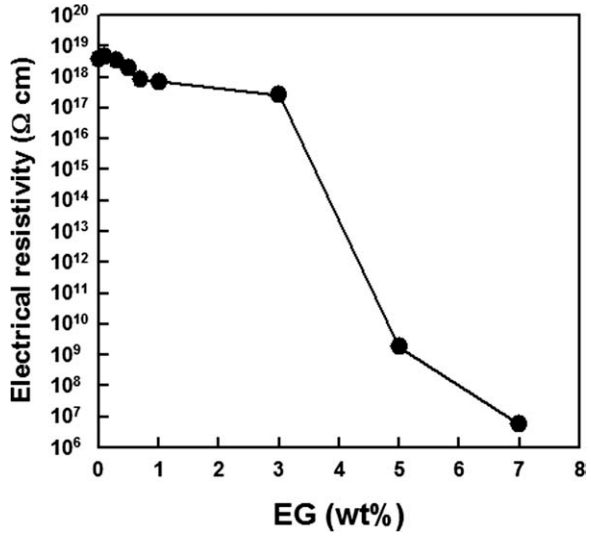

Figure 9 Electrical volume resistivities of PBT/EG nanocomposites as a function of EG content.

film was evaluated to be in the order of $\sim 10^{18}$ Ω cm. This result supports that PBT is a typical electrically insulating material. In cases of the nanocomposites, the electrical volume resistivity slightly decreased with the increment of the EG content up to ~ 3 wt % graphene and also there was a dramatic decrease in electrical resistivity at certain EG content between 3 and 5 wt %. This substantial reduction in the electrical resistivity is associated with the formation of the electrical conduction path. When the EG content reaches a percolation threshold between 3 and 5 wt % EG, the distance among graphene platelets in the matrix is close enough in a few nanometer ranges for the electrical conduction via the electron hopping mechanism.[44,45] Thus, the electrical volume resistivity of the nanocomposite with 7.0 wt % EG content is achieved to be $\sim 10^6$ Ω cm. It is noticeable that the nanocomposites with the low electrical resistivity of $\sim 10^6$ Ω cm can be used for thermoplastic applications requiring the electrostatic dissipation and partial electromagnetic insulation.[46] In the meantime, it might be interesting to compare the electrical resistivities of PBT-based composites including EG or carbon black (CB). In case of PBT/CB composites, it was reported that the electrical percolation is achieved at certain CB content between 4 and 6 wt %,[47] which is a slightly higher conductive filler content when compared with PBT/EG nanocomposites in this study. It is usual that CB-loaded static controlling composites contain 10~ 20 wt % CB, resulting from the relatively low surface-to-volume ratio of CB. Therefore, it is speculated that the slightly lower percolation threshold concentration in PBT/EG nanocomposites stems from the high surface-to-volume ratio of EG, compared with CB.

CONCLUSIONS

In this study, a series of PBT nanocomposites reinforced with graphene platelets of EG were manufactured via the melt-compounding method. SEM images and X-ray diffraction patterns confirmed that the graphene platelets of EG were well dispersed and remained exfoliated in the PBT matrix, even for the nanocomposite with high EG content of 7.0 wt %. Raman spectroscopic analysis confirmed that there exists an aromatic–aromatic interaction between phenyl rings of PBT chains and graphene platelets of EG at the interface of nanocomposites. DSC cooling and heating thermograms showed that the graphene platelets in the nanocomposites induced the formation of thicker and more stable PBT α-phase crystals and also promoted the overall melt-crystallization of PBT. This result indicated that the graphene platelets of EG acted as nucleating agents for the formation of PBT α-phase crystals due to the favorable interaction between graphene platelets and PBT chains. Thermo-oxidative stability of PBT/EG nanocomposites was found to be improved significantly with the increment of EG content owing to the barrier effect of graphene platelets in the PBT matrix to the permeating oxygen gas. Dynamic storage moduli of the nanocomposites were also enhanced noticeably due to the uniform distribution and good interfacial adhesion of graphene platelets in the PBT matrix. In addition, the electrical volume resistivities of the nanocomposites were changed dramatically from $\sim 10^{18}$ to $\sim 10^6$ Ω cm with increasing the EG content. The percolation threshold for electrical conduction in the PBT/EG nanocomposites was found to be at certain EG content between 3 and 5 wt %. Overall, it was found that graphene platelets of EG affected strongly the structure-processing-property relationship of PBT by accelerating the melt-crystallization rate as well as by enhancing thermo-oxidative stability, mechanical and electrical properties. It is thus considered that PBT/EG nanocomposites can be used as advanced materials in the area requiring improved physical properties.

References

1. Hobbs, S. Y.; Pratt, C. F. J Appl Polym Sci 1975, 19, 1701.
2. Bair, H. E.; Berrington, G. H.; Kelleher, P. G. J Polym Sci Part B: Polym Phys 1976, 14, 2113.
3. Hobbs, S. Y.; Robb, R. C. Polymer 1980, 21, 559.
4. Robeson, L. M. J Polym Sci Part C: Polym Lett 1978, 16, 261.
5. Wahrmund, D. C.; Paul, D. R.; Barlow, J. W. J Appl Polym Sci 1978, 22, 2155.
6. Guo, M. M.; Zachmann, H. G. Macromolecules 1997, 30, 2746.
7. Hale, W. R.; Pessan, L. A.; Keskkula, H.; Paul, D. R. Polymer 1999, 40, 4237.
8. Arostegui, A.; Nazabal, J. Polymer 2003, 44, 5227.
9. Shin, H.; Park, E. S. J Appl Polym Sci 2009, 114, 3008.
10. Walch, E.; Gaymans, R. J. Polymer 1994, 35, 636.

11. Jeong, Y. G.; Jo, W. H.; Lee, S. C. Macromolecules 2000, 33, 9705.
12. Shi, X. Q.; Ito, H.; Kikutani, T. Polymer 2005, 46, 11442.
13. Car, A.; Stropnik, C.; Yave, W.; Peinemann, K. V. Adv Funct Mater 2008, 18, 2815.
14. Stade, K. H. Polym Eng Sci 1978, 18, 107.
15. Gensler, R.; Groppel, P.; Muhrer, V.; Muller, N. Part Syst Char 2002, 19, 293.
16. Acierno, D.; Scarfato, P.; Amendola, E.; Nocerino, G.; Costa, G. Polym Eng Sci 2004, 44, 1012.
17. Broza, G.; Kwiatkowska, M.; Roslaniec, Z.; Schulte, K. Polymer 2005, 46, 5860.
18. Novoselov, K. S.; Geim, A. K.; Morozov, S. V.; Jiang, D.; Zhang, Y.; Dubonos, S. V.; Grigorieva, I. V.; Firsov, A. A. Science 2004, 306, 666.
19. Zhang, Y.; Tan, Y. -W.; Stomer, H. L.; Kim, P. Nature 2005, 438, 201.
20. Lee, C.; Wei, X.; Kysar, J. W.; Hone, J. Science 2008, 321, 385.
21. Stankovich, S.; Dikin, D. A.; Dommett, G. H. B.; Kohlhaas, K. M.; Zimney, E. J.; Stach, E. A.; Piner, R. D.; Nguyen, S. T.; Ruoff, R. S. Nature 2006, 442, 282.
22. Yasmin, A.; Luo, J. -J.; Daniel, I. M. Compos Sci Technol 2006, 66, 1182.
23. Kalaitzidou, K.; Fukushima, H.; Drzal, L. T. Compos Sci Technol 2007, 67, 2045.
24. Ramanathan, T.; Abdala, A. A.; Stankovich, S.; Dikin, D. A.; Herrera-Alonso, M.; Piner, R. D.; Adamson, D. H.; Schniepp, H. C.; Chen, X.; Ruoff, R. S.; Nguyen, S. T.; Aksay, I. A.; Prudhomme, R. K.; Brinson, L. C. Nat Nanotech 2008, 3, 327.
25. Rafiee, M.; Rafiee, J.; Wang, Z.; Song, H.; Yu, Z. -Z.; Koratkar, N. ACS Nano 2009, 3, 3884.
26. Pramoda, K. P.; Linh, N. T. T.; Tang, P. S.; Tjiu, W. C.; Goh, S. H.; He, C. B. Compos Sci Technol 2010, 70, 578.
27. Zhao, X.; Zhang, Q.; Chen, D.; Lu, P. Macromolecules 2010, 43, 2357.
28. Kim, H.; Abdala, A. A.; Macosko, C. W. Macromolecules 2010, 43, 6515.
29. Potts, J. R.; Dreyer, D. R.; Bielawski, C. W.; Ruoff, R. S. Polymer 2011, 52, 5.
30. Staudenmaier, L. Ber Dtsch Bot Ges 1898, 31, 1481.
31. Schniepp, H. C.; Li, J. -L.; McAllister, M. J.; Sai, H.; Herrera-Alonso, M.; Adamson, D. H.; Prudhomme, R. K.; Car, R.; Saville, D. A.; Aksay, I. A. J Phys Chem B. 2006, 110, 8535.
32. McAllister, M. J.; Li, J. -L.; Adamson, D. H.; Schniepp, H. C.; Abdala, A. A.; Liu, J.; Herrera-Alonso, M.; Milius, D. L.; Car, R.; Prudhomme, R. K.; Aksay, I. A. Chem Mater 2007, 19, 4396.
33. Kim, I. -H.; Jeong, Y. G. J Polym Sci Part B: Polym Phys 2010, 48, 850.
34. Jakeways, R.; Smith, T.; Ward, I. M.; Wilding, M. A. J Polym Sci Part C: Polym Lett 1976, 14, 41.
35. Hall, I. H.; Pass, M. G. Polymer 1976, 17, 807.
36. Yokouchi, M.; Sakakibara, Y.; Chatani, Y.; Tadokoro, H.; Tanaka, T.; Yoda, K. Macromolecules 1976, 9, 266.
37. Tashiro, K.; Nakai, Y.; Kobayashi, M.; Tadokoro, H. Macromolecules 1980, 13, 137.
38. Pimenta, M. A.; Dresselhaus, G.; Dresselhaus, M. S.; Cancago, L. G.; Jorio, A.; Saito, R. Phys Chem Chem Phys 2007, 9, 1276.
39. Ward, I. M.; Wilding, M. A. Polymer 1977, 18, 327.
40. Wakabayashi, K.; Brunner, P. J.; Masuda, J.; Hewlett, S. A.; Torkelson, J. M. Polymer 2010, 51, 5525.
41. Nichols, M. E.; Robertson, R. E. J Polym Sci Part B: Polym Phys 1992, 30, 305.
42. Kim, H.; Miura, Y.; Macosko, C. W. Chem Mater 2010, 22, 3441.
43. Halpin, J. C.; Kardos, J. L. Polym Eng Sci 1976, 16, 344.
44. Li, C.; Thostenson, E. T.; Chou, T. -W. Appl Phys Lett 2007, 91, 223114.
45. Potschke, P.; Abdel-Goad, M.; Pegel, S.; Jehnichen, D.; Mark, J. E.; Zhou, D. H.; Heinrich, G. J Macromol Sci Part A: Pure Appl Chem 2010, 47, 12.
46. Moniruzzaman, M.; Winey, K. I. Macromolecules 2006, 39, 5194.
47. Narkis, M.; Lidor, G.; Vaxman, A.; Zuri, L. J Electrostat 1999, 47, 201.